Enhancement of Ti_3C_2 MXene Pseudocapacitance after Urea Intercalation Studied by Soft X-ray Absorption Spectroscopy

*Ameer Al-Temimy[1,2] *, Babak Anasori[3,4], Katherine A. Mazzio[1], Florian Kronast[1], Mykola Seredych[3], Narendra Kurra[3], Mohamad-Assaad Mawass[1], Simone Raoux[1,5], Yury Gogotsi[3], and Tristan Petit[1] **

[1] Helmholtz-Zentrum Berlin für Materialien und Energie GmbH, Albert-Einstein-Str. 15, 12489 Berlin, Germany
[2] Department of Physics, Freie Universität Berlin, Arnimallee 14, 14195 Berlin, Germany
[3] Department of Materials Science and Engineering, and A. J. Drexel Nanomaterials Institute, Drexel University, Philadelphia, PA 19104, USA
[4] Department of Mechanical and Energy Engineering, Integrated Nanosystems Development Institute, Purdue School of Engineering and Technology, Indiana University–Purdue University Indianapolis, Indianapolis, IN 46202, USA
[5]Institute of Physics, Humboldt University Berlin, Newtonstr. 15, 12489 Berlin, Germany

Email: ameer.al-temimy@helmholtz-berlin.de, tristan.petit@helmholtz-berlin.de

Abstract

MXenes have shown outstanding properties due to their highly active hydrophilic surfaces coupled with high metallic conductivity. Many applications rely on the intercalation between $Ti_3C_2T_x$ (T_x describes the surface termination) flakes by ions or molecules, which in turn might alter the $Ti_3C_2T_x$ surface chemistry and electrochemical properties. In this work, we show that the capacitance, rate capability, and charge carrier kinetics in $Ti_3C_2T_x$ MXene electrodes are remarkably enhanced after urea intercalation (u-$Ti_3C_2T_x$). In particular, the areal capacitance increased to 1100 mF/cm^2, which is a 56% higher than that of pristine $Ti_3C_2T_x$ electrodes. We attribute this dramatic improvement to changes in the $Ti_3C_2T_x$ surface chemistry upon urea intercalation. The oxidation state and the oxygen bonding of individual $Ti_3C_2T_x$ flakes before and after urea intercalation was probed by soft X-ray absorption spectroscopy (XAS) at the Ti L- and O K-edges with 30 nm spatial resolution in vacuum. After urea intercalation, a higher Ti oxidation state was observed across the entire flake compared to pristine $Ti_3C_2T_x$. Additionally, *in situ* XAS of u-$Ti_3C_2T_x$ aqueous dispersions revealed a higher Ti oxidation similar to dry samples, while for pristine $Ti_3C_2T_x$ the Ti atoms are significantly reduced in water compared to dry samples.

Introduction

Electrochemical energy storage (EES) systems with high capacitance, fast rate capabilities, and low-cost electrodes are urgently demanded as society transitions to sustainable energy technologies. MXenes are a class of 2D transition metal carbides, nitrides, and carbonitrides that are currently attracting considerable attention for EES purposes.[1–6] MXenes combine high electrical conductivity with hydrophilic 2D lamellas, enabling the fast and reversible insertion of a variety of intercalants in organic or aqueous environments.[7–9] Intercalation of MXenes

was found to have an impact on their surface chemistry and was suggested as a strategy to obtain higher pseudocapacitance performance.[10] MXenes can be intercalated both chemically and electrochemically by mono- and multivalent metal cations such as H^+, Li^+, Na^+, K^+, and Mg^{2+}, as well as by organic molecules such as hydrazine.[3,11–13] Recently, an outstanding urea adsorption capacity was demonstrated in $Ti_3C_2T_x$ MXenes, suggesting that these materials could be promising for use in wearable kidneys.[14] Urea intercalation has also been applied as a first step to generate nitrogen-doped $Ti_3C_2T_x$ MXenes with improved capacitance in aqueous electrolyte.[15]

The MXene interlayer distance has been found to be directly proportional to the intercalant's hydration size, and intercalation generally induces a larger spacing between the material layers, as demonstrated by X-ray diffraction (XRD).[16] Despite the relatively large size of urea compared to the interlayer gallery of MXenes, the change in the interlayer distance after intercalation is relatively small owing to the parallel orientation of urea molecules relative to the MXene surface, regardless of the possible surface terminations, T_x.[14] In another study, the decomposition temperature of urea was shown to be reduced to ~60 °C when intercalated into MXenes.[17] The impact of urea intercalation on the surface chemistry of pristine $Ti_3C_2T_x$ MXene and on the electrolyte's ion transportation mechanism remains largely unexplored, while they represent a cornerstone in pseudocapacitance performance.

Soft X-ray Absorption Spectroscopy (XAS)[1,6,18] is an element-selective technique that is very sensitive to surface chemistry. In particular, the characterization of transition metal L-edges is very sensitive to the metal chemical environment and has been used to distinguish the various Ti oxide species.[19,20] While previous XAS reports on $Ti_3C_2T_x$ MXenes at the Ti K-edge have shown changes of Ti oxidation state during cycling in different conditions,[1,6] Ti L-edge can provide further information on the nature of the chemical bonds between Ti atoms and surface groups due to its higher sensitivity to metal-ligand coordination.[21] However, the shorter penetration depth of soft X-rays makes *in situ* experiments on thick electrodes much more complicated at the Ti L-edge compared to the Ti K-edge. Furthermore XAS can be acquired using X-ray Photoemission Electron Microscopy (X-PEEM) to provide XA spectra with 30 nm spatial resolution in vacuum.[22] Pristine $Ti_3C_2T_x$ MXenes have also been found to be sensitive to oxidation due to a charge transfer that can take place between surface O and Ti atoms.[23,24] The high chemical sensitivity of XAS at the Ti L-edge can also be employed *in situ* in aqueous environments using flow cells with thin X-ray transparent membranes.[20] Probing the MXene Ti chemical environment in different environments is important as electrochemical reactions take place in aqueous media. Nevertheless, XAS in the soft X-ray range has not been applied on MXene so far.

In this work, we characterized the electrochemical performance of pristine and urea-intercalated $Ti_3C_2T_x$ (u-$Ti_3C_2T_x$) MXene electrodes and correlated it to the nature of Ti-O bonding probed in vacuum and in water using XAS at the Ti L- and O K-edges. Spatially-resolved oxidation over individual $Ti_3C_2T_x$ MXene flakes was characterized by X-PEEM. In addition, *in*

situ XAS was performed on aqueous dispersions of MXenes to observe the effect of solvation on MXene electronic structure. The u-$Ti_3C_2T_x$ MXenes were characterized under similar conditions and demonstrated a significantly higher Ti oxidation state and capacitance compared to the pristine $Ti_3C_2T_x$ MXene. The u-$Ti_3C_2T_x$-based electrode exhibits enhanced capacitance performance and rate capabilities over pristine $Ti_3C_2T_x$ electrodes, the origin of which will be discussed based on XAS characterization in this work.

Experimental section

Materials: $Ti_3C_2T_x$ MXenes were synthesized from the respective precursor Ti_3AlC_2. To make $Ti_3C_2T_x$, 1 g of Ti_3AlC_2 (<37 µm particle size) powder was added into 10 mL of 10% hydrofluoric acid (50%, Fisher Scientific) solution for 2 min. The solution was stirred for 24 h at 35 °C. The obtained multilayered $Ti_3C_2T_x$ was repeatedly washed with deionized water, followed by centrifugation and decantation until the pH of the suspension reached ~6. After the final centrifugation, the sediment of each $Ti_3C_2T_x$ MXene was collected via vacuum-assisted filtration, and the obtained $Ti_3C_2T_x$ powder was kept under vacuum at room temperature to prevent any deterioration due to oxidation. To study the impact of urea intercalation on the $Ti_3C_2T_x$ MXene, the adsorption of urea was performed in aqueous solution with an initial urea concentration of 5 g/dL at room temperature. 2 g of MXene ($Ti_3C_2T_x$) powder was added to 50 mL of aqueous urea solution and mixed by hand for approximately 6 min, followed by shaking at 150 rpm for an hour. Afterwards, the $Ti_3C_2T_x$/urea suspension was centrifuged at 1000 rpm for 2 min. Both the precipitate and supernatant were reserved for analysis. The resulting u-$Ti_3C_2T_x$ precipitate and the pristine $Ti_3C_2T_x$ precipitate were dried via vacuum-assisted filtration and used for XRD analysis. Both samples were also vacuum annealed at 110 °C for 12 hours (marked as @ 110 °C) to remove any intercalated water prior to performing XRD analysis. For other experiments than XRD, the samples were not annealed prior characterization.

Thermogravimetric analysis-mass spectrometry (TG-MS): TG-MS measurements were carried out using a TA Instruments thermal analyzer (SDT Q 650, Discovery Series) equipped with a Mass Spectrometer (110/220V) from room temperature to 1000°C with a heating rate of 10 °C/min under a constant helium flow 100 mL/min. The gas products that evolved during heating were determined by MS and mass/charge (m/z) evolution profiles as a function of temperature were obtained. The ion current was normalized by the corresponding initial weight of the materials loaded for TG-MS analysis.

X-PEEM and TEY-XAS measurements in vacuum: All sample preparation and thin film processing for synchrotron measurements were carried out in the chemistry laboratory at the Energy Materials *In situ* Laboratory Berlin (EMIL), jointly operated by Helmholtz-Zentrum Berlin für Materialien and Energie, GmbH (HZB) and the Max-Planck Society. Solid samples were spin coated in air on conductive Si substrates to obtain isolated multi-layer single flakes of pristine $Ti_3C_2T_x$, u-$Ti_3C_2T_x$, and a thin TiO_2 nanoparticle film. In order to mimic the studied bulk like sample, we have investigated the oxidation state of Ti atoms of relatively thick flake with more or less the same flake size. Please note that this is quite difficult with XPEEM

technique as it took hours just to find a good candidate flake. The samples were characterized by XAS using Partial Electron Yield (PEY) mode with the X-PEEM endstation at the UE-49-PGM-A beamline of the synchrotron light source BESSY II operated by HZB. Anatase TiO_2 nanoparticles (PL-TiO, Plasmachem, GmbH) have an average particle size of 4–8 nm and were stabilized by a 10 wt% nitric acid (HNO_3) solution. Drop cast films on conductive Si substrates for all samples were dried in air first and then measured in Total Electron Yield (TEY) mode under vacuum conditions at the U49-2_PGM1 beamline of BESSY II using the LiXEdrom endstation.

***In situ XAS measurements in water*:** Experiments were conducted at the U49-2_PGM1 undulator beamline of BESSY II using the LiXEdrom endstation. Pure water, dispersed multilayered $Ti_3C_2T_x$, u-$Ti_3C_2T_x$, and 1M urea in water samples were characterized using a membrane-based flow cell using Total Fluorescence Yield (TFY) recorded with a XUV-100 silicon photodiode (AMS Technologies). 50 nm thick silicon nitride membranes (Plano GmbH) with a window size of 0.5mm x 0.5mm were used to isolate the liquid from the vacuum chamber (10^{-6} mbar range), which is required for soft XAS measurements. To have a constant flow during the experiments enabling efficient sample renewal during measurement, a Legato 270 syringe pump (KD Scientific Inc.) was operated in push-pull mode with a flow rate of 1 mL/min. After characterization of each sample, the flow cell was flushed with deionized water and reference spectra were acquired again at the O K-edge to validate that no sample contamination was left in the cell.
The energy of the O K-edge was calibrated to the water pre-edge at 535.0 eV. For clarity, the intensity of the O K edge XA spectra was normalized to the intensities before and after the water main edge. The Ti L-edge was normalized to the dried $Ti_3C_2T_x$ MXene L_3 (t_{2g}) peak at 458.1 eV.

Electrochemical measurements:

- *MXene and activated carbon (AC) electrode films*

Multilayer powders of $Ti_3C_2T_x$ or u-$Ti_3C_2T_x$ were mixed with polytetrafluoroethylene (60 wt.% in water, Sigma Aldrich) to form a weight ratio of 95:5 for the working electrode films. Similarly, activated carbon (AC) films were prepared by mixing 5 wt.% polytetrafluoroethylene (60 wt.% in water, Sigma Aldrich) with 95 wt.% YP50 (Kuraray, Japan). Electrodes were formed by rolling the mixtures into 100 µm thick films followed by drying in a vacuum oven at 70 °C overnight.

The electrochemical tests (cyclic voltammetry, galvanostatic charge-discharge, electrochemical impedance spectra) were conducted at room temperature using a VMP3 electrochemical workstation (BioLogic, France). Cyclic voltammograms (CV) were recorded using a VMP3 at scan rates ranging from 5-100 mV/s after pre-cycling electrodes at 5 mV/s for 50 cycles. Electrochemical impedance spectroscopy (EIS) measurements were performed in the frequency range from 100 kHz to 0.1 Hz at open circuit potential by applying a small

sinusoidal potential signal with an amplitude of 10 mV. The 3-electrode measurements were performed in 1M H_2SO_4 electrolyte, in which $Ti_3C_2T_x$ and u-$Ti_3C_2T_x$ electrodes were employed as the working electrodes with over-capacitive activated carbon and Ag/AgCl as the counter and reference electrodes, respectively. Gravimetric, areal, and volumetric capacitances were calculated based on the weight, area, and volume of the active materials, respectively.

- *Calculations*

The gravimetric specific capacitance, C_m (F/g), of the electrode materials was calculated from the CV curves by integrating the discharge portion according to the following equation:

$C_m = \frac{1}{\mathrm{V}mv} \int idV$ where *i* is the current (mA), *V* is the potential window (V), v is the scan rate (mV/s), and *m* is the mass of the active material (mg).

Areal capacitance values (F/cm^2) C_A were estimated by multiplying the gravimetric capacitance with the areal mass loading (~ 20 mg/cm^2) of the working electrodes.

$C_A = C_m * mass\ loading$

Volumetric capacitance (F/cm^3) values were estimated by normalizing the areal capacitance with the thickness (100 µm) of the working electrodes

$C_V = C_A / thickness$

Results and Discussion

$Ti_3C_2T_x$ MXenes were synthesized via the 10 wt.% hydrofluoric acid (HF) selective etching method[25] and urea intercalation was performed according to previously published methods (see SI for details).[25] **Figure 1a** illustrates a schematic of the urea intercalation in $Ti_3C_2T_x$ MXenes. The orientation of urea molecules in the gallery of the MXene flakes shown in Figure 1a is based on our previous computational calculations.[14] XRD patterns of the as-synthesized pristine $Ti_3C_2T_x$ and the u-$Ti_3C_2T_x$ at room temperature are shown in **Figure 1b**. The u-$Ti_3C_2T_x$ sample shows a 002 diffraction peak at 7° 2θ (corresponding to a *c* lattice parameter of 25.3 Å), which corresponds well with the *c* lattice parameter expected for urea intercalated in a planar orientation as shown in **Figure 1a**.[14] However, a similar spacing was also observed for the pristine MXene as a result of water intercalation.[26] We therefore performed vacuum annealing at 110 °C to remove intercalated water molecules in both samples. The 002 peak shifted to 8.6° 2θ and 6.4° 2θ for pristine $Ti_3C_2T_x$ and the u-$Ti_3C_2T_x$, corresponding to *c* lattice parameters of ~20.6 and ~27.6 Å, respectively. The interlayer spacing of pristine $Ti_3C_2T_x$ clearly decreases upon water desorption, which is not observed for u-$Ti_3C_2T_x$. This indicates that the large interlayer spacing for u-$Ti_3C_2T_x$ at room temperature is not due to water intercalation. The difference in spacing between the two annealed MXene samples (~3.5 Å) is similar to that of a previously reported change in kaolinite interlayer spacing after urea intercalation.[27]
To shed light on the nature of the intercalated species, TG-MS measurements were performed (**Figure 1c**). Our results show decomposition products from urea starting from 130 °C,

representing a ~3.4 wt.% loss, demonstrating that urea was present in the u-$Ti_3C_2T_x$ at room temperature. The TG-MS results also show that the interlayer water that exists in pristine $Ti_3C_2T_x$ was largely replaced by urea molecules due to the difference in water weight loss from 2% for pristine $Ti_3C_2T_x$ to <0.2% in u-$Ti_3C_2T_x$. As the sample environment was dissimilar during the XRD and TG-MS measurements, there is a possibility that urea had already decomposed prior to the XRD measurements performed at 110 °C in vacuum, as has been suggested in a previous study.[17] This will be studied in detail in future work. Irrespective of the urea stability at high temperature, both XRD and TG-MS measurements demonstrate that urea was intercalated in u-$Ti_3C_2T_x$ at room temperature.

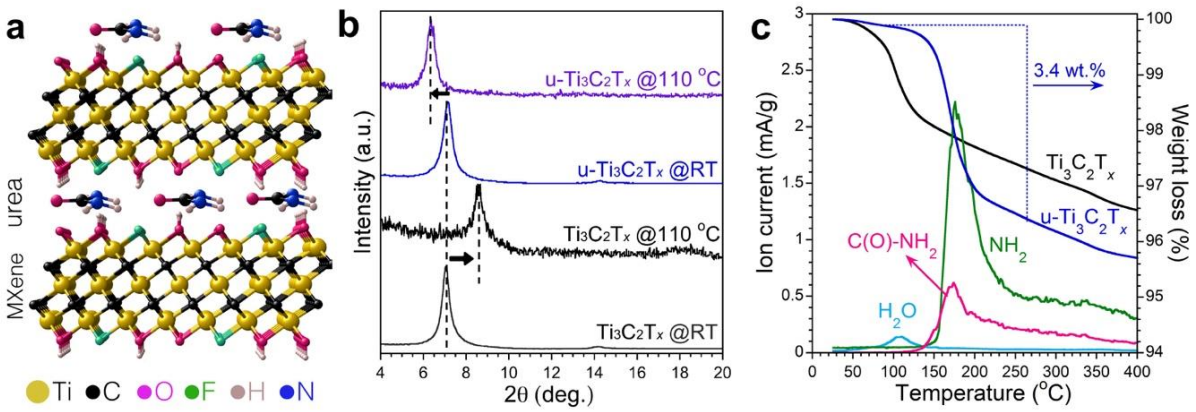

Figure 1. (a) Schematic of urea adsorption on $Ti_3C_2T_x$ from an aqueous urea solution. (b) X-ray diffraction patterns of the as-synthesized $Ti_3C_2T_x$ powder at room temperature ($Ti_3C_2T_x$ @RT) and after annealing at 110 °C ($Ti_3C_2T_x$ @110 °C), $Ti_3C_2T_x$ after urea adsorption at room temperature (u-$Ti_3C_2T_x$ @RT) and after annealing at 110 °C (u-$Ti_3C_2T_x$ @ 110°C). The arrows show the change in position of the 002 diffraction peaks after vacuum annealing at 110 °C. (c) Thermogravimetric analysis for pristine $Ti_3C_2T_x$ and u-$Ti_3C_2T_x$, and mass spectrometry from the u-$Ti_3C_2T_x$.

The electrochemical behavior of $Ti_3C_2T_x$ and u-$Ti_3C_2T_x$ MXenes was investigated using three-electrode cells assembled in 1M H_2SO_4 electrolyte (see SI). **Figure 2a** shows typical cyclic voltammograms of u-$Ti_3C_2T_x$ and $Ti_3C_2T_x$ electrodes at a scan rate of 5 mV/s. The broad redox envelop is more prominent in the case of u-$Ti_3C_2T_x$ compared to $Ti_3C_2T_x$, which can be attributed to the increased accessibility of protons and hydronium ions within the MXene galleries after the intercalation of urea molecules. Interestingly, there is a small reduction peak at -0.51 V (vs. Ag/AgCl) for the u-$Ti_3C_2T_x$ electrode, which is absent in the case of $Ti_3C_2T_x$. This is probably due to the protonation of urea molecules at low scan rates, as a reduction peak at high scan rates (>20 mV/s) is absent, as shown in **Figure S2**. The areal (volumetric) capacitance of u-$Ti_3C_2T_x$ increases dramatically, and is found to be 1100 mF/cm^2 (110 F/cm^3), which is 56% higher compared to pristine $Ti_3C_2T_x$ electrodes. Please note that the volumetric capacitance of u-$Ti_3C_2T_x$ electrodes (ultrathick electrodes, ~100 µm at mass loading of 20 mg/cm^2) should not be compared with the few micron thick MXene electrodes (~1-5 µm at mass loading of 1-3 mg/cm^2) reported by Lukatskaya et al.[28] as the investigated electrode here is powder-based rather than a freestanding film electrode. Optimization of the electrode capacitance in terms of absolute numbers is currently in progress.

The rate retention capability of u-$Ti_3C_2T_x$ is superior relative to $Ti_3C_2T_x$ as shown in **Figure 2b**. These findings corroborate with the measured XRD, where the enlarged interlayer spacing of u-$Ti_3C_2T_x$ provides not only a greater number of electrochemically active sites, but also facilitates much faster diffusion of electrolyte ions relative to $Ti_3C_2T_x$ electrodes. Likewise, charge-discharge profiles at a current density of 1.5 A/g reveal higher capacitance for u-$Ti_3C_2T_x$ relative to $Ti_3C_2T_x$, as illustrated in **Figure 2c**. Importantly, the u-$Ti_3C_2T_x$ electrode exhibits superior ion transport kinetics relative to $Ti_3C_2T_x$. Figure 4d shows the electrochemical impedance data of $Ti_3C_2T_x$ and u-$Ti_3C_2T_x$ MXenes which supports the good capacitive and rate performance of urea intercalated $Ti_3C_2T_x$. The inset in **Figure 2d** highlights the absence of a semi-circle and 45° line in the high frequency region for the u-$Ti_3C_2T_x$ electrode, indicating a more efficient mass diffusion.

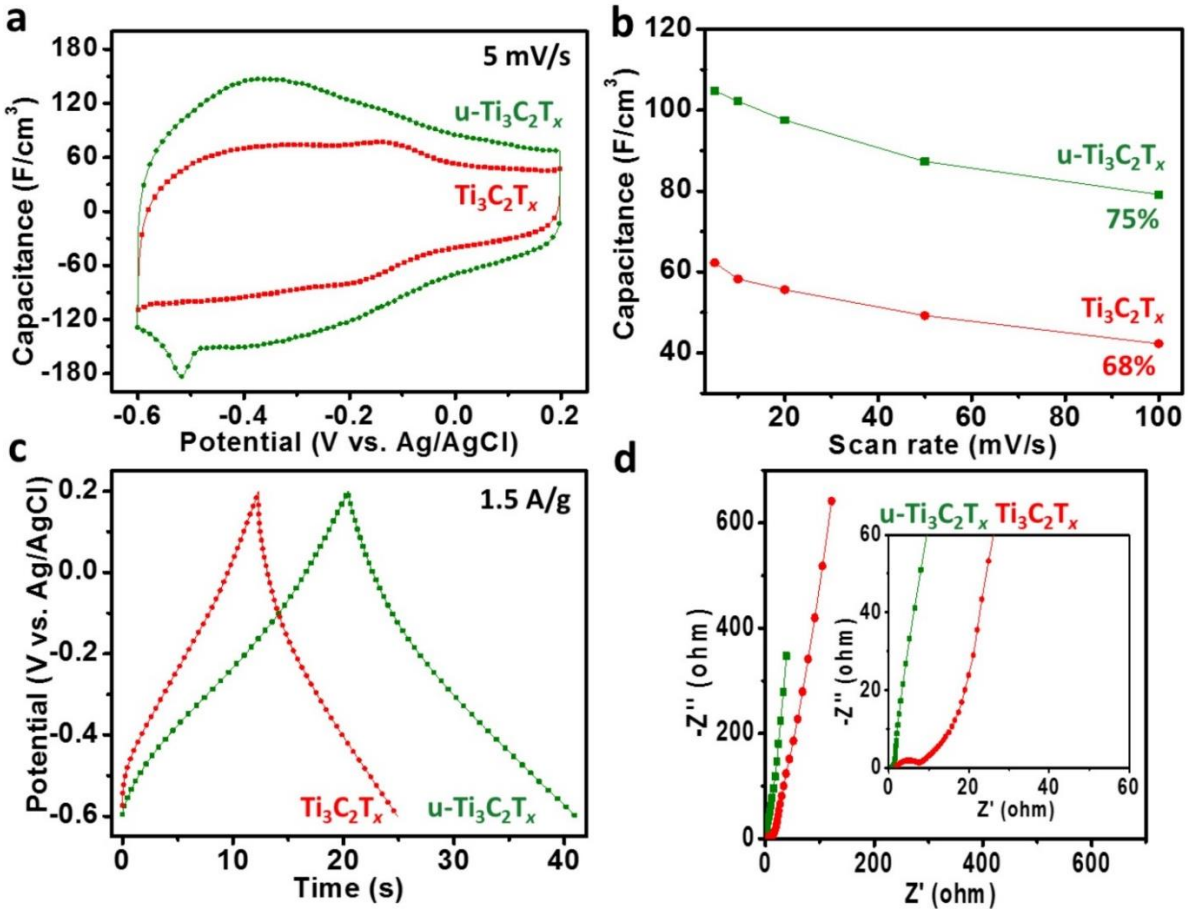

Figure 2. Comparison of the electrochemical performance between $Ti_3C_2T_x$ and u-$Ti_3C_2T_x$ electrodes in 1M H_2SO_4 electrolyte. (a) Cyclic voltammograms at 5 mV/s. (b) Volumetric capacitance versus scan rate shows 75% retention in u-$Ti_3C_2T_x$ relative to 68% for $Ti_3C_2T_x$ electrodes at 100mV/s scan rate. (c) Galvanostatic charge-discharge profiles at a current density of 1.5 A/g, (d) Electrochemical impedance spectra of MXene electrodes at various frequency regimes.

The oxidation state of the Ti atoms in $Ti_3C_2T_x$ constitutes a key element in the electrochemical performance. To investigate the oxidation state of the Ti atoms, the XAS technique was applied before and after urea intercalation in different environments. **Figure 3a** shows X-PEEM images taken in vacuum at the Ti L-edge of individual $Ti_3C_2T_x$ MXene flakes before and after urea intercalation. The flakes were found to be a few micrometers in diameter, with sharp edges. The yellow and green marked areas in **Figure 3a** serve to highlight the specific regions

denoted as center and edge, respectively, from which XA spectra of the Ti L-edge were extracted from the spectral images. The Ti L-edge is related to the excitation of Ti $2P_{3/2}$ (L_3-edge) and Ti $2P_{1/2}$ (L_2-edge) core levels to an unoccupied Ti 3d state. Due to the ligand field induced by binding with oxygen, the Ti L_3 and L_2 edges are each split into two sub peaks, corresponding to electronic states with t_{2g} and e_g symmetries. The e_g band is known to be highly sensitive to the local environment because the Ti e_g orbitals point directly to the 2p orbitals of the surrounding O atoms.[29,30]

For the $Ti_3C_2T_x$ MXene flake, the splitting of the L_3 edge into t_{2g} and e_g sub-bands was observed at each location on the flake but is more defined at the edge. The onset of the Ti L-edge, shown in **Figure 3b**, also varies between the edge and the center of the flake and is used to estimate the Ti oxidation state. The onset energy shifts from 454.6 eV at the center compared to 455.0 eV at the edge of the flake, corresponding to an estimated oxidation state slightly higher than Ti^{3+} at the center while the edge position is relatively close to Ti^{4+} (see **Figure S3a**).

For the u-$Ti_3C_2T_x$ MXene flake, the X-PEEM-based XAS reveals that the L_3 feature splits into two pronounced sub-bands corresponding to the t_{2g} and e_g peaks. The pre-edge onset energy of 455.8 eV is independent of location on the u-$Ti_3C_2T_x$ flake and corresponds to a large Ti^{4+}contribution. The Ti atoms are in a significantly higher state of oxidation relative to the pristine $Ti_3C_2T_x$ MXene flake and are homogeneously oxidized over the entire flake.

The oxygen distribution and local bonding environment were also characterized by X-PEEM at the O K-edge. To better visualize the oxygen distribution across the flake, X-PEEM difference images are shown in **Figure 3c**. A higher contrast close to the flake edges demonstrates a higher oxygen content in this region for the pristine MXene, while the oxygen content appears more homogeneous after urea intercalation (see also **Figure S4**). **Figure S5** shows that the oxygen content on pristine $Ti_3C_2T_x$ is mostly concentrated in the first few hundreds of nanometers from the edge. **Figure 3d** shows a comparison of O K-edge XA spectra for pristine $Ti_3C_2T_x$ and u-$Ti_3C_2T_x$ MXenes at the center and edge positions of the flakes. The O K-edge XAS exhibit two main peaks in the energy range between 529.0-535.0 eV which originate from the transitions between oxygen 1s and 2p states that are hybridized with empty Ti 3d orbitals. Furthermore, the O K-edge spectra also show a second set of bands in the energy region from 537.0-546.0 eV, which can be assigned to transitions from O 2p states that are hybridized with Ti 4s and 4p states.[31] The MXene spectral features at 530.8 and 533.2 eV are assigned to the t_{2g} and e_g orbitals, respectively. However, for the pristine $Ti_3C_2T_x$, the e_g peak intensity was found to be relatively low in the center, suggesting a lower average oxidation state there relative to the edges.

After urea intercalation, the e_g peak at 533.2 eV becomes well-resolved, as shown in **Figure 3d**. The O K-edge spectra thus emphasize the similar oxidation state across the u-$Ti_3C_2T_x$ MXene flake, which agrees with the Ti L-edge results (see also **Figure S3b**). Note that the contribution of intercalated urea is possibly appearing between 532.5 and 534.0 eV. The features observed between 537.0-540.0 eV at the u-$Ti_3C_2T_x$ edge position are attributed to the SiO_2 substrate (**Figure S6**).

The higher level of Ti oxidation state at the edges of the pristine $Ti_3C_2T_x$ MXene can probably be explained by its higher exposure to water molecules and oxygen from the ambient environment during aqueous dispersion and drying in air. Indeed, the oxidation proceeds faster at the edge positions of a $Ti_3C_2T_x$ flake relative to the basal plane, which has been found to eventually contribute to an overall decrease in conductivity of MXene electrodes.[32–35]

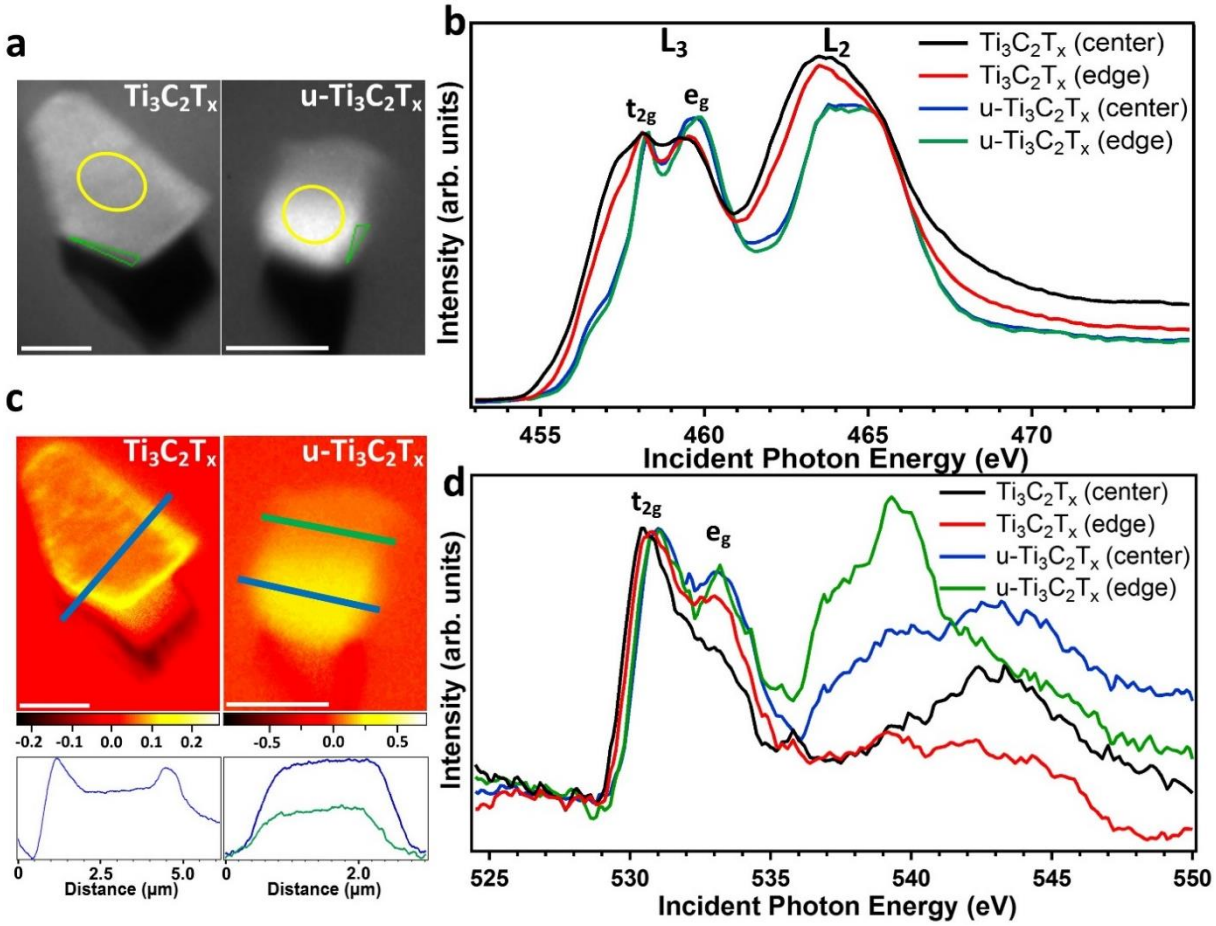

Figure 3. (a) X-PEEM micrographs at the Ti L-edge taken at an excitation energy of 463.9 eV (black and white) show individual flakes of pristine $Ti_3C_2T_x$ and u-$Ti_3C_2T_x$ MXenes (scale bar 2 µm). The regions labeled center and edge in (b, d) are highlighted in yellow and green, respectively. (b) X-PEEM Ti L-edge XA spectra of single flakes of pristine $Ti_3C_2T_x$ and u-$Ti_3C_2T_x$ MXenes. (c) Oxygen content distribution over individual MXene flakes obtained from the difference of averaged X-PEEM micrographs at the O K-edge in the t_{2g} and e_g region (530.0-534.5 eV) relative to the background (524.5-529.0 eV), the corresponding line profiles across the flake are shown underneath. (d) X-PEEM O K-edge XA spectra of pristine $Ti_3C_2T_x$ and u-$Ti_3C_2T_x$ MXene samples.

As the oxidation state of MXenes strongly influences their redox properties and despite a high Ti oxidation state (close to 4+) after urea intercalation, u-$Ti_3C_2T_x$ electrodes exhibit a reversible redox reaction as is evident from the broad redox profile shown earlier in **Figure 2a**. In order to estimate the origin of the increased Ti oxidation, *in situ* XAS measurements were also directly performed in water. The effect of aqueous solvation on the Ti oxidation state of the MXenes were monitored by comparing the Ti L-edge XA spectra of dried and dispersed pristine $Ti_3C_2T_x$ MXene multilayered powders (**Figure 4**). For the $Ti_3C_2T_x$ powder dried in air and then

characterized under vacuum, the Ti L_3-edge includes a peak around 458.1 eV and a shoulder at about 459.4 eV which confirms the coexistence of different Ti species, while the Ti L_2-edge shows a single peak at about 463.4 eV. The XA spectra of the dried $Ti_3C_2T_x$ MXene sample, averaged over a large number of flakes, are very similar to the X-PEEM spectra recorded for individual flakes. On the other hand, the dispersed $Ti_3C_2T_x$ MXene shows no splitting of the Ti L_3-edge into t_{2g} and e_g states, and a broad peak is detected at 457.4 eV. This new feature is shifted by -0.7 eV compared to the maximum of the L_3 peaks of dried $Ti_3C_2T_x$ sample, indicating a lower level of the oxidation state. Estimation of the Ti oxidation state from the pre-edge onset suggests a contribution from Ti^{2+} species for the dispersed sample (**Figure S 3b**).[19,36]

For u-$Ti_3C_2T_x$ samples, the Ti L-edge XA spectra have similar profiles in both dry and solvated environments, as depicted in **Figure 4**. The $L_{2,3}$ edges split into two components separated by about 5.4 eV. The Ti L_2-edge (462.3- 467.6 eV) features are broadened relative to the Ti L_3-edge (457.3-461.3 eV) features, and are similar to previous reports on TiO_2 materials.[29] The e_g peaks are broader than the t_{2g} peaks which can be attributed to a larger degree of hybridization of the Ti e_g orbitals with O orbitals.[37] Unlike the pristine $Ti_3C_2T_x$ MXenes, the surface Ti atoms in both dried and solvated u-$Ti_3C_2T_x$ MXenes have an averaged oxidation state close to Ti^{4+}, like in TiO_2. O K-edge XAS was also performed for $Ti_3C_2T_x$ and u-$Ti_3C_2T_x$ MXenes dispersed in water, which supports the higher oxygen bonding to Ti atoms on u-$Ti_3C_2T_x$ MXenes (see **Figure S7**).

These results demonstrate that the oxidation state of the Ti atoms of the pristine $Ti_3C_2T_x$ samples varies with the sample environment. The averaged Ti oxidation state of the dried $Ti_3C_2T_x$ MXene was found to be close to the Ti^{3+} species, similar to X-PEEM results. On the other hand, dispersed $Ti_3C_2T_x$ in water shows a significant contribution from Ti^{2+} species, which is probably induced by a significant increase of hydroxyl groups at the MXene surface after dispersion in water, inducing a reduction of Ti oxidation state. No clear e_g peak is observed at the L_3-edges as opposed to the dry sample, showing that no Ti-O bonds with a strong σ-character are detected in water. The same sample has been used for these experiments so that pristine $Ti_3C_2T_x$ MXene may be slightly oxidized upon drying in air.[32] As a result, $Ti_3C_2(OH)_2$ terminations may change to $Ti_3C_2O_2$ terminations, resulting in an increase in the Ti oxidation state to Ti^{3+}.

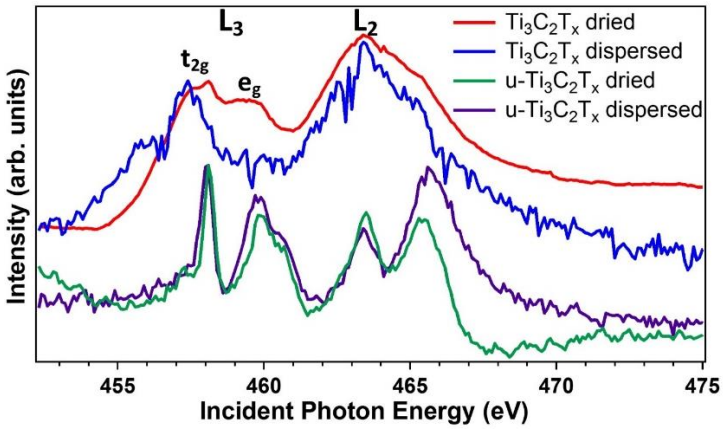

Figure 4. Ti L-edge XA spectra of dried and dispersed pristine $Ti_3C_2T_x$ and u-$Ti_3C_2T_x$ MXenes. Dispersed samples in water were characterized by XAS in Total Fluorescence Yield (TFY) mode using a flow cell and dried samples in Total Electron Yield (TEY) mode in vacuum.

In contrast, Ti atoms of the u-$Ti_3C_2T_x$ MXene appear highly oxidized both in water and after drying with an estimated average Ti oxidation state very close to Ti^{4+}. It is worth noting that the higher Ti oxidation state does not mean that the MXene samples are transformed into TiO_2 as no signature from TiO_2 is evident by the full XRD pattern shown in **Figure S1**.

Shedding light on the difference in the MXene oxidation state and surface chemistry after urea intercalation requires a thorough understanding of the intercalation mechanism. The interlayer distance of the $Ti_3C_2T_x$ planes after urea intercalation is similar but results from different intercalated molecules (water or urea, **Figure 1b**), and thus less van der Waals and hydrogen bonding between the layers.[38] Owing to the size of urea, the urea molecules might occupy considerable space within the interlayer distances between the MXene sheets with a preference of parallel orientation to the MXene surface.[14] The increased MXene interlayer spacing may facilitate the bonding of oxygen, possibly coming from urea molecules, to the Ti atoms, and thus a higher Ti oxidation state is observed. On the other hand, the strong interaction between urea molecules and the Ti atoms on the MXene surface[14] would likely prevent hydroxylation of the surface Ti atoms upon dispersion in water. Higher oxidation occurs over the entire MXene flake for u-$Ti_3C_2T_x$, while only the edges are relatively oxidized in the pristine $Ti_3C_2T_x$ MXene. The higher Ti oxidation of u-$Ti_3C_2T_x$ is apparently not reversible after dispersion in water. The higher oxidation of surface Ti atoms after urea intercalation is most probably related to the observed higher pseudocapacitance. The latter is in full agreement with previous work on TiO_2-Ti_3C_2 nanocomposites showing a capacitance about 54% higher relative to pristine $Ti_3C_2T_x$ electrodes.[39] Furthermore, another study revealed that having more oxidized surface group in $Ti_3C_2T_x$ MXene lead to enhanced electrochemical performance.[40]

Conclusion

In summary, the areal capacitance of multilayered u-$Ti_3C_2T_x$ powder-based electrodes is found to be 1100 mF/cm^2, reflecting a 56% increase compared to pristine $Ti_3C_2T_x$ electrodes.

Interestingly, the diffusion of the electrolyte ions in the presence of urea was observed to be very fast. We have probed the chemical environment of Ti atoms of both pristine $Ti_3C_2T_x$ and u-$Ti_3C_2T_x$ MXene samples through XAS-based characterization in vacuum and aqueous dispersions. Despite the high observed Ti oxidation state (close to 4+), induced by covalent bonding with oxygen atoms, reversible redox reactions have been shown in u-$Ti_3C_2T_x$ electrodes as is evident from the broad redox profile. This suggests that a higher metal oxidation state constitutes an opportunity to enhance the electrochemical performance in MXene-based electrodes. The XA spectra at the Ti L- and O K-edges show that the electronic structure of $Ti_3C_2T_x$ is dramatically altered after urea intercalation. Using the high spatial resolution of X-PEEM, a direct mapping of the electronic structure of Ti and O atoms over a single $Ti_3C_2T_x$ flake demonstrated a higher oxidation at the edges compared to the basal plane of the flake while a homogeneous oxidation was detected over the entire u-$Ti_3C_2T_x$ MXene flake. Finally, *in situ* XAS measurements in water demonstrated that hydration is affecting the chemical bonding of Ti atoms in pristine $Ti_3C_2T_x$ MXene. This work illustrates that soft X-ray absorption spectroscopy is a powerful method to probe the electronic structure of transition metal oxide surface of MXenes in various environments. It paves the way to further investigations on MXene surface chemistry, especially after intercalation with various compounds or cations.

Acknowledgments

A.A. acknowledges the German Academic Exchange Service (DAAD) for financial support during the PhD. A.A. and T.P. acknowledge the financial support from the Volkswagen Foundation (Freigeist Fellowship No. 89592). A.A. is grateful for the extra fund support from HZB by Prof. Simone Raoux and DAAD devoted for short term research stay at Drexel University, PA in USA. We acknowledge Dr. Qi Zhao, Dr. Narendra Kurra, and Dr. Christopher Shuck for helping us in some of the XRD measurements. The authors acknowledge the kind support by staff members of the BESSY II synchrotron facility especially the beamline scientists at beamline UE-49-PGM-A and beamline U49-2_PGM1 at BESSY II. We thank HZB for the allocation of synchrotron radiation beamtime.

Supporting Information Available: Full XRD patterns, Scan-rate dependent cyclic voltammograms, details on Ti oxidation state estimation, X-PEEM and in situ XAS at the O K edge.

Author contributions

The manuscript was written by A.A. with contributions from all coauthors. A.A. and T.P. designed and conducted the XAS measurements, and A.A. performed the entire data analysis. A.A., K.A.M., F.K., and S.R. planned the X-PEEM experiments. A.A., K.A.M., F.K., M.A.M and S.R. performed the X-PEEM experiments. B.A. and M.S. conducted the material synthesis, XRD, and TG-MS measurements. A.A., T.P. and S.R. planned the electrochemical performance measurements and it was conducted by N.K. and A.A. S.R., Y.G., and T.P. supervised the research.

Conflict of Interest

The authors declare no conflict of interest.

References

(1) Lukatskaya, M. R.; Bak, S.-M.; Yu, X.; Yang, X.-Q.; Barsoum, M. W.; Gogotsi, Y. Probing the Mechanism of High Capacitance in 2D Titanium Carbide Using In Situ X-Ray Absorption Spectroscopy. *Adv. Energy Mater.* **2015**, *5* (15), 1500589. https://doi.org/10.1002/aenm.201500589.

(2) Anasori, B.; Lukatskaya, M. R.; Gogotsi, Y. 2D Metal Carbides and Nitrides (MXenes) for Energy Storage. *Nat. Rev. Mater.* **2017**, *2* (2), 16098. https://doi.org/10.1038/natrevmats.2016.98.

(3) Lukatskaya, M. R.; Mashtalir, O.; Ren, C. E.; Dall'Agnese, Y.; Rozier, P.; Taberna, P. L.; Naguib, M.; Simon, P.; Barsoum, M. W.; Gogotsi, Y. Cation Intercalation and High Volumetric Capacitance of Two-Dimensional Titanium Carbide. *Science* **2013**, *341* (6153), 1502–1505. https://doi.org/10.1126/science.1241488.

(4) Eames, C.; Islam, M. S. Ion Intercalation into Two-Dimensional Transition-Metal Carbides: Global Screening for New High-Capacity Battery Materials. *J. Am. Chem. Soc.* **2014**. https://doi.org/10.1021/ja508154e.

(5) Naguib, M.; Come, J.; Dyatkin, B.; Presser, V.; Taberna, P. L.; Simon, P.; Barsoum, M. W.; Gogotsi, Y. MXene: A Promising Transition Metal Carbide Anode for Lithium-Ion Batteries. *Electrochem. commun.* **2012**. https://doi.org/10.1016/j.elecom.2012.01.002.

(6) Xie, Y.; Naguib, M.; Mochalin, V. N.; Barsoum, M. W.; Gogotsi, Y.; Yu, X.; Nam, K. W.; Yang, X. Q.; Kolesnikov, A. I.; Kent, P. R. C. Role of Surface Structure on Li-Ion Energy Storage Capacity of Two-Dimensional Transition-Metal Carbides. *J. Am. Chem. Soc.* **2014**, *136* (17), 6385–6394.

(7) Wang, X.; Kajiyama, S.; Iinuma, H.; Hosono, E.; Oro, S.; Moriguchi, I.; Okubo, M.; Yamada, A. Pseudocapacitance of MXene Nanosheets for High-Power Sodium-Ion Hybrid Capacitors. *Nat. Commun.* **2015**. https://doi.org/10.1038/ncomms7544.

(8) Luo, J.; Zhang, W.; Yuan, H.; Jin, C.; Zhang, L.; Huang, H.; Liang, C.; Xia, Y.; Zhang, J.; Gan, Y.; et al. Pillared Structure Design of MXene with Ultralarge Interlayer Spacing for High-Performance Lithium-Ion Capacitors. *ACS Nano* **2017**, *11* (3), 2459–2469.

(9) Gao, Y.; Wang, L.; Li, Z.; Zhang, Y.; Xing, B.; Zhang, C.; Zhou, A. Electrochemical Performance of Ti_3C_2 Supercapacitors in KOH Electrolyte. *J. Adv. Ceram.* **2015**. https://doi.org/10.1007/s40145-015-0143-3.

(10) Li, J.; Yuan, X.; Lin, C.; Yang, Y.; Xu, L.; Du, X.; Xie, J.; Lin, J.; Sun, J. Achieving High Pseudocapacitance of 2D Titanium Carbide (MXene) by Cation Intercalation and Surface Modification. *Adv. Energy Mater.* **2017**, *7* (15).

(11) Mashtalir, O.; Lukatskaya, M. R.; Zhao, M. Q.; Barsoum, M. W.; Gogotsi, Y. Amine-Assisted Delamination of Nb_2C MXene for Li-Ion Energy Storage Devices. *Adv. Mater.* **2015**, *27* (23), 3501–3506.

(12) Mashtalir, O.; Naguib, M.; Mochalin, V. N.; Dall'Agnese, Y.; Heon, M.; Barsoum, M. W.; Gogotsi, Y. Intercalation and Delamination of Layered Carbides and Carbonitrides. *Nat. Commun.* **2013**. https://doi.org/10.1038/ncomms2664.

(13) Naguib, M.; Unocic, R. R.; Armstrong, B. L.; Nanda, J. Large-Scale Delamination of Multi-Layers Transition Metal Carbides and Carbonitrides "MXenes." *Dalt. Trans.* **2015**. https://doi.org/10.1039/c5dt01247c.

(14) Meng, F.; Seredych, M.; Chen, C.; Gura, V.; Mikhalovsky, S.; Sandeman, S.; Ingavle, G.; Ozulumba, T.; Miao, L.; Anasori, B.; et al. MXene Sorbents for Removal of Urea from Dialysate: A Step toward the Wearable Artificial Kidney. *ACS Nano* **2018**, *12*, 10518–10528.

(15) Yang, C.; Que, W.; Yin, X.; Tian, Y.; Yang, Y.; Que, M. Improved Capacitance of Nitrogen-Doped Delaminated Two-Dimensional Titanium Carbide by Urea-Assisted Synthesis. *Electrochim. Acta* **2017**, *225*, 416–424.

(16) Ghidiu, M.; Halim, J.; Kota, S.; Bish, D.; Gogotsi, Y.; Barsoum, M. W. Ion-Exchange and Cation Solvation Reactions in Ti_3C_2 MXene. *Chem. Mater.* **2016**, *28* (10), 3507–3514.

(17) Overbury, S. H.; Kolesnikov, A. I.; Brown, G. M.; Zhang, Z.; Nair, G. S.; Sacci, R. L.; Lotfi, R.; Van Duin, A. C. T.; Naguib, M. Complexity of Intercalation in MXenes: Destabilization of Urea by Two-Dimensional Titanium Carbide. *J. Am. Chem. Soc.* **2018**. https://doi.org/10.1021/jacs.8b05913.

(18) Bak, S. M.; Qiao, R.; Yang, W.; Lee, S.; Yu, X.; Anasori, B.; Lee, H.; Gogotsi, Y.; Yang, X. Q. Na-Ion Intercalation and Charge Storage Mechanism in 2D Vanadium Carbide. *Adv. Energy Mater.* **2017**, *7* (20), 1700959.

(19) Stoyanov, E.; Langenhorst, F.; Steinle-Neumann, G. The Effect of Valence State and Site Geometry on Ti $L_{3,2}$ and O K Electron Energy-Loss Spectra of Ti_xO_y Phases. *Am. Mineral.* **2007**, *92* (4), 577–586.

(20) Petit, T.; Ren, J.; Choudhury, S.; Golnak, R.; Lalithambika, S. S. N.; Tesch, M. F.; Xiao, J.; Aziz, E. F. X-Ray Absorption Spectroscopy of TiO_2 Nanoparticles in Water Using a Holey Membrane-Based Flow Cell. *Adv. Mater. Interfaces* **2017**, *4* (23), 1700755. https://doi.org/10.1002/admi.201700755.

(21) Baker, M. L.; Mara, M. W.; Yan, J. J.; Hodgson, K. O.; Hedman, B.; Solomon, E. I. K- and L-Edge X-Ray Absorption Spectroscopy (XAS) and Resonant Inelastic X-Ray Scattering (RIXS) Determination of Differential Orbital Covalency (DOC) of Transition Metal Sites. *Coord. Chem. Rev.* **2017**, *345*, 182–208. https://doi.org/10.1016/J.CCR.2017.02.004.

(22) Kronast, F.; Valencia Molina, S. SPEEM: The Photoemission Microscope at the Dedicated Microfocus PGM Beamline UE49-PGMa at BESSY II. *J. large-scale Res. Facil. JLSRF* **2016**. https://doi.org/10.17815/jlsrf-2-86.

(23) Karlsson, L. H.; Birch, J.; Halim, J.; Barsoum, M. W.; Persson, P. O. Å. Atomically Resolved Structural and Chemical Investigation of Single MXene Sheets. *Nano Lett.*

2015, *15* (8), 4955–4960. https://doi.org/10.1021/acs.nanolett.5b00737.

(24) Gan, L. Y.; Huang, D.; Schwingenschlögl, U. Oxygen Adsorption and Dissociation during the Oxidation of Monolayer Ti_2C. *J. Mater. Chem. A* **2013**, *1* (43), 13672–13678.

(25) Alhabeb, M.; Maleski, K.; Anasori, B.; Lelyukh, P.; Clark, L.; Sin, S.; Gogotsi, Y. Guidelines for Synthesis and Processing of Two-Dimensional Titanium Carbide ($Ti_3C_2T_x$ MXene). *Chem. Mater.* **2017**, *29* (18), 7633–7644.

(26) Fredrickson, K. D.; Anasori, B.; Seh, Z. W.; Gogotsi, Y.; Vojvodic, A. Effects of Applied Potential and Water Intercalation on the Surface Chemistry of Ti_2C and Mo_2C MXenes. *J. Phys. Chem. C* **2016**. https://doi.org/10.1021/acs.jpcc.6b09109.

(27) Zhang, S.; Liu, Q.; Gao, F.; Li, X.; Liu, C.; Li, H.; Boyd, S. A.; Johnston, C. T.; Teppen, B. J. Mechanism Associated with Kaolinite Intercalation with Urea: Combination of Infrared Spectroscopy and Molecular Dynamics Simulation Studies. *J. Phys. Chem. C* **2017**, *121* (1), 402–409. https://doi.org/10.1021/acs.jpcc.6b10533.

(28) Lukatskaya, M. R.; Kota, S.; Lin, Z.; Zhao, M.-Q. Q.; Shpigel, N.; Levi, M. D.; Halim, J.; Taberna, P.-L. L.; Barsoum, M. W.; Simon, P.; et al. Ultra-High-Rate Pseudocapacitive Energy Storage in Two-Dimensional Transition Metal Carbides. *Nat. Energy* **2017**, No. 2, 17105. https://doi.org/10.1038/nenergy.2017.105.

(29) Kucheyev, S. O.; van Buuren, T.; Baumann, T. F.; Satcher, J. H.; Willey, T. M.; Meulenberg, R. W.; Felter, T. E.; Poco, J. F.; Gammon, S. A.; Terminello, L. J. Electronic Structure of Titania Aerogels from Soft X-Ray Absorption Spectroscopy. *Phys. Rev. B* **2004**, *69* (24), 245102. https://doi.org/10.1103/PhysRevB.69.245102.

(30) Hsu, M.-Y.; Yang, W.-C.; Teng, H.; Leu, J. Microstructure and Composition of TiO_2 Nanotube Arrays Fabricated with HF and NH_4F Electrolytes and Their Evolution during Annealing. *J. Electrochem. Soc.* **2011**. https://doi.org/10.1149/1.3533388.

(31) De Groot, F. M. F.; Grioni, M.; Fuggle, J. C.; Ghijsen, J.; Sawatzky, G. A.; Petersen, H. Oxygen 1s X-Ray-Absorption Edges of Transition-Metal Oxides. *Phys. Rev. B* **1989**. https://doi.org/10.1103/PhysRevB.40.5715.

(32) Lipatov, A.; Alhabeb, M.; Lukatskaya, M. R.; Boson, A.; Gogotsi, Y.; Sinitskii, A. Effect of Synthesis on Quality, Electronic Properties and Environmental Stability of Individual Monolayer Ti3C2MXene Flakes. *Adv. Electron. Mater.* **2016**. https://doi.org/10.1002/aelm.201600255.

(33) Zhang, C. J.; Pinilla, S.; McEvoy, N.; Cullen, C. P.; Anasori, B.; Long, E.; Park, S. H.; Seral-Ascaso, A.; Shmeliov, A.; Krishnan, D.; et al. Oxidation Stability of Colloidal Two-Dimensional Titanium Carbides (MXenes). *Chem. Mater.* **2017**, *29* (11), 4848–4856.

(34) Lotfi, R.; Naguib, M.; Yilmaz, D. E.; Nanda, J.; Van Duin, A. C. T. A Comparative Study on the Oxidation of Two-Dimensional Ti_3C_2 MXene Structures in Different Environments. *J. Mater. Chem. A* **2018**, *6* (26), 12733–12743.

(35) Chertopalov, S.; Mochalin, V. N. Environment-Sensitive Photoresponse of Spontaneously Partially Oxidized Ti_3C_2 MXene Thin Films. *ACS Nano* **2018**, *12* (6), 6109–6116.

(36) Zhan, C.; Naguib, M.; Lukatskaya, M.; Kent, P. R. C. C.; Gogotsi, Y.; Jiang, D. E.

Understanding the MXene Pseudocapacitance. **2018**, *9* (6), 1223–1228. https://doi.org/10.1021/acs.jpclett.8b00200.

(37) De Groot, F. M. F.; Faber, J.; Michiels, J. J. M.; Czyyk, M. T.; Abbate, M.; Fuggle, J. C. Oxygen 1s X-Ray Absorption of Tetravalent Titanium Oxides: A Comparison with Single-Particle Calculations. *Phys. Rev. B* **1993**. https://doi.org/10.1103/PhysRevB.48.2074.

(38) Naguib, M.; Mochalin, V. N.; Barsoum, M. W.; Gogotsi, Y. 25th Anniversary Article: MXenes: A New Family of Two-Dimensional Materials. *Adv. Mater.* **2014**, *26* (7), 992–1005.

(39) Zhu, J. F.; Tang, Y.; Yang, C. H.; Wang, F.; Cao, M. J. Composites of TiO_2 Nanoparticles Deposited on Ti_3C_2 Mxene Nanosheets with Enhanced Electrochemical Performance. *J. Electrochem. Soc.* **2016**, *163* (5), A785–A791.

(40) Hu, M.; Hu, T.; Li, Z.; Yang, Y.; Cheng, R.; Yang, J.; Cui, C.; Wang, X. Surface Functional Groups and Interlayer Water Determine the Electrochemical Capacitance of $Ti_3C_2T_x$ MXene. *ACS Nano* **2018**, *12* (4), 3578–3586. https://doi.org/10.1021/acsnano.8b00676.

TOC Graphic

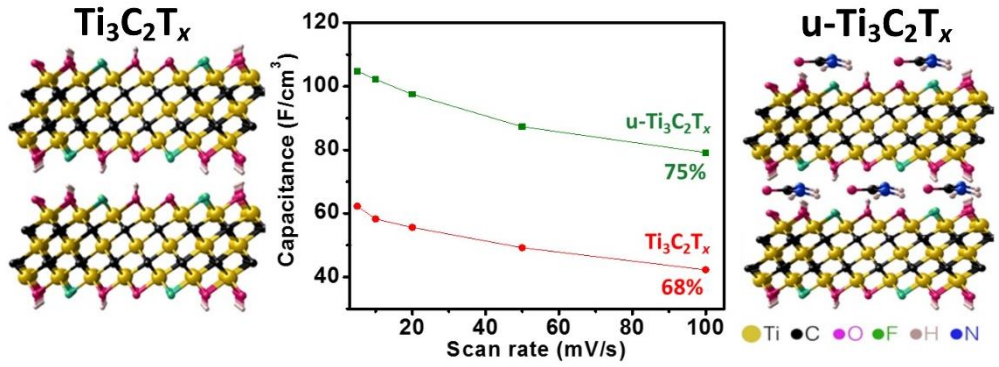
Ti3C2Tx
120
100
80
60
40
Capacitance (F/cm3)
u-Ti3C2Tx
75%
Ti3C2Tx
68%
20
40
60
80
100
Scan rate (mV/s)
u-Ti3C2Tx
Ti C O F H N